Terrestrial, Atmospheric and Oceanic Sciences

RESEARCH Open Access

Fast report: Coseismic source model of the January 2025 M_w 6.1 Dapu earthquake from geodetic data and its implications for seismogenic structures in Southwestern Taiwan

Yogendra Sharma[1*], Kuo-En Ching[1], Wu-Lung Chang[2], He-Chin Chen[3], Shih-Han Hsiao[1], Wu-Yu Liao[4], En-Jui Lee[4], Ray Y. Chuang[5] and Chien-Liang Chen[6]

Abstract

In southwestern Taiwan, the longstanding debate between thin-skinned and thick-skinned models is exemplified by the 2025 M_w ~6.1 Dapu earthquake, especially considering its proximity to the 1964 Mw ~ 6.5 Baihe earthquake. Joint GNSS–InSAR analysis and early aftershock distribution reveal a predominantly east-dipping reverse fault, with high slip at depths of 8–15 km as a single asperity. The maximum coseismic of 40 cm is located at ~ 12 km depth. The estimated seismic moment release along the source fault is 1.49×10^{25} dyne-cm equivalent to a M_w 6.08 earthquake. Further, the subsequent seismic activity suggests that a west-dipping fault was also triggered, underscoring the complexity of conjugate fault systems extending into deeper levels of the fold-and-thrust belt. This geometry, defined by detailed seismic, geodetic, and focal mechanism data, indicates that basement-involved deformation occurs well beneath the traditionally proposed thin-skinned décollement, highlighting the importance of thick-skinned processes in regional tectonics. Coulomb stress modeling shows a 0.2–0.3 MPa stress increase contiguous to the coseismic slip area, suggesting the potential for future seismic activity on nearby faults. Meanwhile, high-pressure fluid zones at shallow depths may encourage aseismic creep, mitigating seismic hazards at the surface but shifting major rupture potential to deeper locked segments. These findings underscore the critical role of basement-involved faults in the tectonic framework of southwestern Taiwan and emphasize the need for continued, integrated geophysical monitoring to refine seismic hazard assessments.

*Correspondence:
Yogendra Sharma
yogenmaths2738@gmail.com
[1]Department of Geomatics, National Cheng Kung University, No. 1, Dasyue Road, East District, Tainan 701, Taiwan
[2]Department of Earth Sciences, National Central University, Taoyuan, Taiwan
[3]National Land Surveying and Mapping Center, Ministry of the Interior, Taichung, Taiwan
[4]Department of Earth Sciences, National Cheng Kung University, Tainan, Taiwan
[5]Department of Geography, National Taiwan University, Taipei, Taiwan
[6]Geological Survey and Mining Management Agency, Ministry of Economic Affairs, Taipei, Taiwan

1 Introduction

A M_w 6.1 earthquake at a depth of 15 km struck regions near Dapu township in southwestern Taiwan on 21 January 2025 (Taiwan time), followed by more than 100 aftershocks within 24 h of the mainshock, including two M_w > 5.0 events (Wu et al. 2025). According to the Central Weather Administration (CWA) of Taiwan, this region has been known to host devastating earthquakes, for example, the 1906 M7.1 Meishan earthquake, the 1941 M7.2 Chungpu earthquake, and the 1964 M6.3 Baihe earthquake. In particular, the hypocenter of this Dapu earthquake nearly coincides with that of the Baihe earthquake which occurred at a depth of 18 km (Peng et al. 2019). Further, the Baihe earthquake and the aftershock distribution of the Dapu earthquake indicate that the source fault could be located below the décollement (Le Béon et al. 2024). Because determining the location of seismogenic faults is key to seismic hazard assessment, establishing an accurate structural fault model for southwestern Taiwan is important. This raises the question of whether deeper, basement-involved faults below the décollement play a significant role in this region's seismicity.

The classical tectonic model of southwest Taiwan presumes a thin-skinned system, where deformation is primarily accommodated by shallow thrust faults above a major décollement (Wu et al., 1997; Suppe 1980; 1983; Le Béon et al. 2024). However, the main distribution of seismicity deeper than the proposed décollement cannot be explained by the thin-skinned model. A thick-skinned tectonic model, involving deeper crustal faulting and basement-involved deformation, was suggested to explain certain seismic characteristics in this region (Mouthereau et al. 2001; Mouthereau and Lacombe 2006; Ching et al. 2011, 2016; Huang et al. 2016). However, the precise geometry of these basement-involved structures remains largely uncertain, hindering a thorough understanding of seismic hazards in the region. The occurrence of the Dapu earthquake and its ruptured characteristics therefore provide crucial insights into the ongoing debate between these two models.

In the present work, we utilized a combination of 48 continuous GNSS observations (Fig. 1) and Sentinel-1 ascending and descending tracks (Fig. 2) to understand the coseismic deformation pattern associated with the Dapu earthquake. We used the aftershock distribution of the Dapu event from Liao et al. (2025) to define the source fault. Further, the coseismic source model was derived from GNSS and InSAR data based on the given modeled fault plane. Such an integrated geodetic approach provides high-resolution constraints on the coseismic deformation and fault geometry, which are critical for assessing whether the event supports a thin-skinned or thick-skinned structural model.

2 Coseismic surface displacements

2.1 GNSS data

Continuous GNSS observations in the source area were collected from stations by the Geological Survey and Mining Management Agency, mainly operated by the Central Weather Bureau Administration, Academia Sinica, and other organizations. These stations are distributed within ~50 km radius of the epicenter. The GNSS data were processed using the GipsyX software with the precise point positioning method under ITRF2020, achieving sub-centimeter accuracy (Lee et al. 2025).

To quantify the coseismic displacements (Fig. 1), coordinate differences were computed between the average positions recorded during the seven days preceding and three days following the Dapu event (Lee et al. 2025) (Fig. 1). The primary coseismic displacements ranging from 5 mm to 23 mm are concentrated between the Liuchia fault (A in Fig. 1) to the west, the Pingchi fault (G in Fig. 1) to the east, and the Tsochen fault (E in Fig. 1) to the south. Station TAPU (~3 km north of the epicenter) shows the largest horizontal displacement of 23 mm toward the northeast and a vertical uplift of 24 mm. Meanwhile, station GS97 (south of the epicenter) exhibits a 16 mm of southwest-directed motion and 8 mm of uplift. Other nearby stations indicate consistent vertical displacement in a range of 6–10 mm.

2.2 InSAR data

To further refine the spatial resolution of deformation, we utilized Sentinel-1 ascending and descending images (IW mode). Four ascending images (track 69: frames 68 and 72) from 9 January 2025 to 21 January 2025 and two descending images (track 105: frame 514) from 11 January 2025 to 23 January 2025 were processed with the TopsApp module of ISCE2. We applied precise orbital data and a 30-m SRTM DEM for co-registration and topography correction. The adaptive filtering and coherence-based phase smoothing were also applied to minimize the noise. The final unwrapped interferograms were then geocoded and converted to Line-of-Sight (LOS) displacement, with positive values indicating motion toward the satellite.

Both ascending and descending interferograms reveal concentrated deformation in the region southwest of the Dapu epicenter, consistent with the GNSS observations among the Liuchia fault (A in Fig. 2), Pingchi fault (G in Fig. 2), and Tsochen fault (E in Fig. 2). The maximum LOS displacement in the ascending data of ~75 mm is located near the epicenter. The descending data indicates a maximum displacement of ~50 mm, also near the epicenter (Fig. 2).

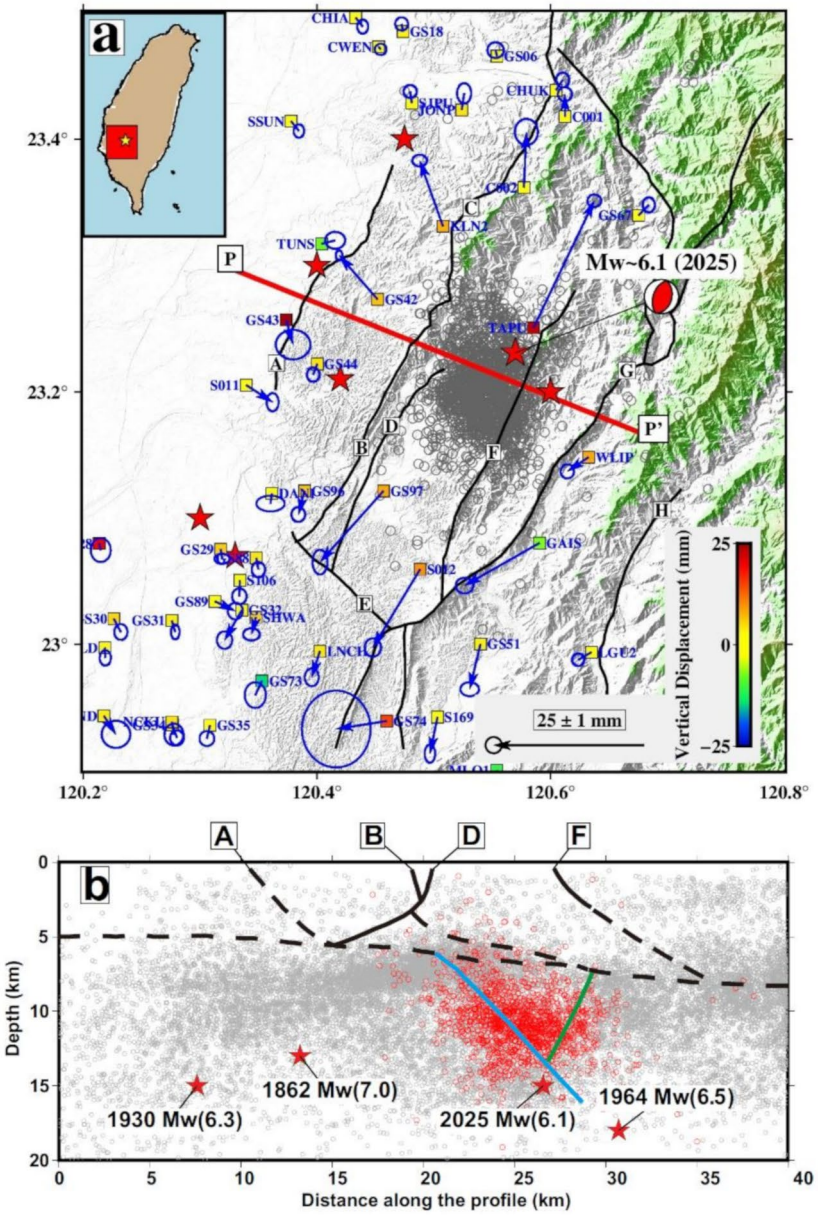

Fig. 1 Seismotectonic of southwest Taiwan. (**a**) The black lines indicate the primary shallow fault system. The gray circles are the aftershocks of the Dapu earthquake. The red star shows the epicenter of historical events and the Dapu earthquake. The arrows indicate the horizontal GNSS displacement 1-sigma uncertainty, whereas the squares are color coded by vertical GNSS displacement. The solid red line (P-P') represents the profile location for Fig. 1b. The red square in the inset shows the boundary of the main figure. A = Liuchia fault; B = Lunhuo Fault; C = Chukou fault; D = Kouhsiaoli fault; E = Tsochen fault; F = Chutouchi fault; G = Pingchi fault; H = Chaozhou fault. (**b**) The structural model in the study area. The black lines represent the fault system (Le Béon et al. 2024). The light blue line is the source fault for the Dapu earthquake. The green line indicates the west-dipping fault. The gray circles represent the background seismicity from 1990 to 2024. The red circles indicate the aftershocks of the Dapu earthquakes. The black dash lines indicate the basal fault system acquired from Le Béon et al. 2024

3 Coseismic source model

According to the temporal and spatial distribution of aftershocks associated with the Dapu earthquake (Liao et al. 2025), the primary source fault is inferred to be east-dipping. To constrain the fault geometry, we examined the aftershock pattern (Fig. 1) and incorporated focal mechanism solutions provided by Taiwan's Real-time Moment Tensor monitoring (RMT) (Lee

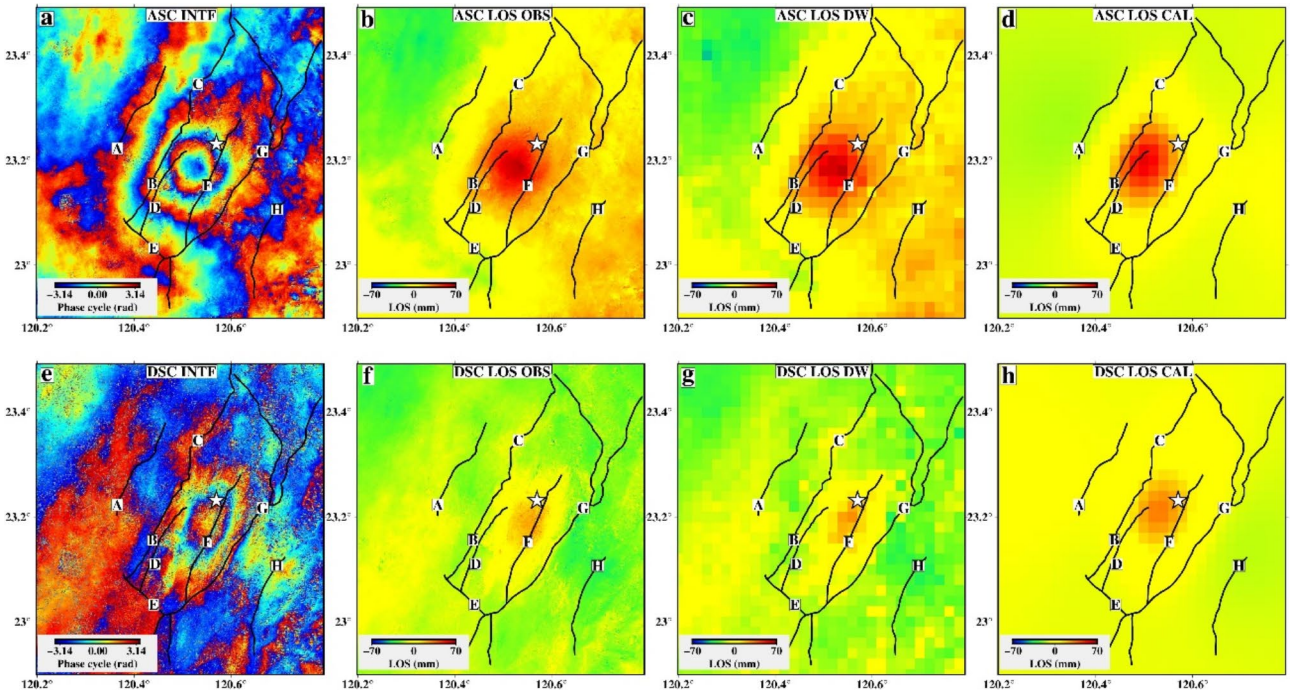

Fig. 2 InSAR displacement during the Dapu earthquake. (**a**) Interferogram ascending image. (**b**) Ascending line-of-sight displacement. (**c**) Downsampled ascending line-of-sight displacement. (**d**) Calculated ascending line-of-sight displacement from the source model. (**e**) Phase cycle from descending image. (**f**) Descending line-of-sight displacement. (**g**) Downsampled descending line-of-sight displacement. (**h**) Calculated descending line-of-sight displacement from the source model. The white star shows the epicenter of the Dapu earthquake, and the black line indicates the fault lines along southwest Taiwan

et al., 2014a, b) and the United States Geological Survey (USGS). Both sources reported nodal planes with dip angles ranging from 39° to 50° (RMT) and 34°to 56° (USGS), and rake angles between 85° to 94°, indicating a predominantly reverse mechanism. Based on these constraints, our modeled fault plane dips 42° to the east, extending from a shallow depth of 6 km down to 16 km (Fig. 1). The fault is modeled with a length of 40 km and a width of 15 km, consistent with the along-strike and along-dip extents of the observed aftershock distribution.

We then used a simple kinematic source model to calculate coseismic slip distribution in a homogeneous elastic half-space (Ching et al. 2007; Okada 1985). The fault plane was divided into 33×10 rectangular patches. We also used a Laplacian smoothing operator to reduce abrupt slip variations between adjacent patches. We inverted the general observation Eq. (1) using least squares estimation (Eq. 2).

$$d = Gs + e \tag{1}$$

$$\min_{s} \frac{1}{2}\left\| \frac{d - Gs}{C} \right\|^2 + \frac{1}{2}\gamma \|Ls\|^2 \tag{2}$$

Here $\boldsymbol{d}$ is the observed displacement vector. $\boldsymbol{G}$ is the design matrix, relating the unknown slip on each fault patch to surface displacements, $\boldsymbol{s}$ is the unknown slip vector on patches, $\boldsymbol{e}$ represents the observational residuals, $\boldsymbol{C}$ is the weighting matrix based on the uncertainty of each observation, $\boldsymbol{L}$ is the Laplacian matrix (designed to penalize large differences between neighboring slip patches), γ is the regularization parameter, controlling the trade-off between data fit and smoothness. We then downsampled the InSAR LOS displacement and significantly reduced the pixel size. We used about 1050 pixels for each ascending and descending track (Fig. 2).

The root-mean-square (RMS) misfit of the optimized model is 16 mm. The inferred coseismic slip is distributed between 8 km and 15 km depth, forming a single asperity centered at ~12 km (Fig. 3). The maximum slip reached 40 cm, indicating near-pure reverse faulting. The coseismic slip is predominantly concentrated southwest of the epicenter, aligning well with the aftershock distribution. We also noticed a shallow slip of 3 cm to 4 cm in the north of the epicenter, between the depth of 6 km to 7 km. This might result from model uncertainty or potential reactivation of shallow structures. Further, the estimated seismic moment release along the source fault is 1.49×10^{25} dyne-cm, corresponding to a moment magnitude (M_w) of 6.08, consistent with the reported M_w 6.1 by Wu et al. (2025). Near-field GNSS displacements match closely with the predicted surface deformation, while the far-field fit is less reliable. This is likely due to local site effects or model complexities in rupture propagation not

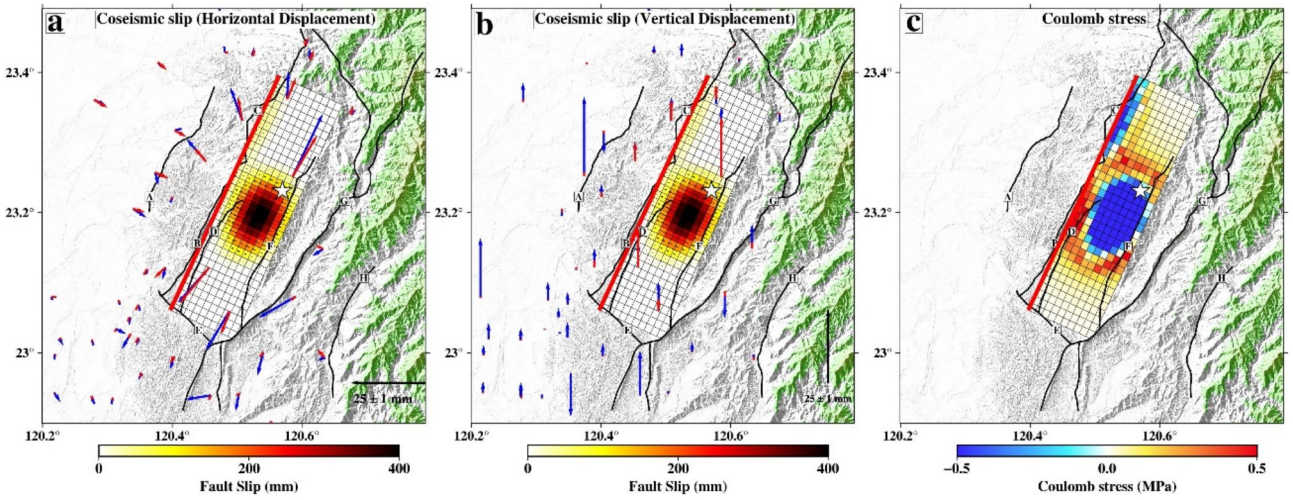

Fig. 3 Coseismic source modeling for the Dapu earthquake. The red line in all the figures indicates the source fault. (**a**) The distribution of coseismic slip during the Dapu earthquake from kinematics source modeling and comparison of observed and modeled horizontal displacement. The blue and red arrows represent the observed and calculated horizontal displacement. (**b**) The comparison of observed and modeled vertical displacement. The blue and red arrows represent the observed and calculated vertical displacement. (**c**) The coulomb stress change induced from the coseismic slip during the Dapu event. The blue color represents stress release, and the red color indicates stress increase

captured by the current model (Fig. 3). Notably, the current fault model is unable to reproduce displacements at several eastern stations (GAIS, WLIP, and GS51), suggesting the possible involvement of additional west-dipping fault segment(s) (Wu et al. 2025; Liao et al. 2025). Similarly, the vertical displacements also show good agreement, with the exception of southern stations GS28, GS43, GS73, and GS74. Moreover, the modeled LOS displacements near the epicenter shows strong consistency (RMS < 16 mm) with both ascending and descending interferograms, further validating the slip distribution.

4 Discussion

4.1 Seismogenic structures in Southwestern Taiwan

The fold-and-thrust belt in southwest Taiwan is widely characterized by a system dominated by east-dipping faults that have developed above a ~ 5-km-deep décollement in the ongoing collision between the Philippine Sea Plate and the Eurasian Plate (Suppe 1984; Teng 1990; Mouthereau et al. 2001). However, a belt of background seismicity located beneath the proposed décollement of the thin-skinned model coincides with the locations of significant historical earthquakes, such as the 1906 Meishan earthquake, the 1941 Chungpu earthquake, and the 1964 Baihe earthquakes. This suggests that deeper fault structures may also contribute to regional tectonic activity (Wu et al. 2010; Brown et al. 2017, 2022). The 2025 Dapu earthquake provides new insights regarding these deeper seismogenic structures.

Our coseismic source modeling, together with the aftershock distribution during the first three hours following the mainshock. suggests that an east-dipping reverse fault served as the major source fault, likely connecting with the Liuchia fault near the surface (Fig. 1b). Subsequently, a west-dipping reverse fault, located ~ 10 km east of the east-dipping fault, was also triggered. The top of this west-dipping fault may intersect the décollement proposed in the thin-skinned model (Fig. 1b). These findings contrast with previous interpretations by Wu et al. (2025) and Liao et al. (2025), who identified the west-dipping fault as the primary source. Because of the multi-day sampling interval of our GNSS and DInSAR data, our model captures the accumulated coseismic slip on the east-dipping fault, although initial nucleation on the west-dipping fault remains possible.

While the east-dipping faults are commonly thought to dominate the structural evolution of the fold-and-thrust belt in southwest Taiwan (Brown et al. 2022; Le Béon et al. 2024; Lin et al. 2025), the west-dipping faults, which act as backthrusts or reactivated faults, also play an important role in its development (Biete et al. 2017; Le Béon et al. 2019; Béon et al. 2024; Brown et al. 2022). In this contest, the conjugated system of east- and west-dipping faults situated above a ~ 5-km-deep décollement is key to the tectonic evolution of the region (Biete et al. 2017; Le Béon et al. 2019; Béon et al. 2024). Similar conjugate fault systems have been documented in other fold-and-thrust belts worldwide, such as in the Himalayas and the Andes (Hubbard et al. 2016; Avouac et al. 2015).

However, our observations from the 2025 Dapu earthquake indicate that conjugate faulting extends well below the depth of 5 km, providing compelling support for a thick-skinned model in this region (Fig. 1b). Clarifying the conjugated geometries of seismogenic faults in the deep crust in this study is very important to improve the seismic hazard assessment in southwestern Taiwan.

4.2 Implication for seismic hazard along Southwest Taiwan

A series of moderate to large earthquakes, including the 2025 Dapu event, has historically struck southwestern Taiwan. However, Le Béon et al. (2024) suggested that the Kouhsiaoli fault in this area is creeping, thereby limiting its ability to accumulate sufficient stress for a large earthquake. One possible mechanism behind this behavior is the presence of abnormally high-pressure zones above ~2 km in depth identified in the CPC drilling data (Yuan et al. 1987). High-pressure fluids within the fault zone could reduce friction and promote the aseismic slip along the shallow portion of the fault plane. Consequently, major earthquakes in this region predominantly nucleate in deeper segments, which remain locked and capable of accumulating the stress necessary for sizable events, as evidenced by the deep slip distribution observed in our Dapu coseismic source model. Recognizing this interplay between high-pressure fluids and aseismic creeping is therefore critical for improving seismic hazard assessments in southwestern Taiwan. Future research should integrate geodetic, seismic, and geological data to further elucidate the depth-dependent behaviors of these faults and to better assess the potential for future large earthquakes.

Based on historical records, the 1964 M_w ~6.5 Baihe earthquake occurred in the same region as the Dapu earthquake, suggesting that larger-magnitude earthquakes remain possible despite the evidence of creeping in the shallow segments. Given that both earthquakes are on the same source fault, the Dapu earthquake may potentially trigger another large earthquake on the same fault. To evaluate the post-Dapu stress state, we conducted a Coulomb stress change analysis, which indicates a 0.2–0.3 MPa stress increase in the surrounding region of the coseismic slip area (Fig. 3c). This increased stress may promote slip on nearby faults, potentially influencing subsequent seismic activity. Indeed, the dense seismic cluster below the Lunhua fault, occurring shortly after the Dapu earthquake (Liao et al. 2025), could reflect partial stress release in the upper side of the fault plane. In light of these findings, ongoing monitoring of fluid pressures, fault creeping, and stress evolution is essential for improving seismic hazard models and understanding how deeper, locked segments might accumulate strain over longer timescales.

5 Conclusions

The 2025 Dapu earthquake has highlighted the contribution of basement-involved faults to the earthquake potential and deformation mechanisms of southwestern Taiwan. Our modeled coseismic slip distribution, centered between 8 km and 15 km depth, supports a thick-skinned deformation regime, with an east-dipping thrust fault acting as the primary rupture plane. However, the subsequent activation of a west-dipping fault underlines the complexity of conjugate fault systems extending to depths > 5 km. The Coulomb stress analysis suggests that stress redistribution following the earthquake may enhance seismic activity on adjacent faults, reinforcing the need to account for multi-fault interactions. While shallow fault segments may exhibit aseismic creep due to high-pressure fluids, deeper zones remain locked, posing a risk of future moderate-to-large earthquakes.

Recognizing this interplay between shallow creep and deeper fault locking is vital for seismic hazard assessment, particularly given the historical record of larger events (e.g., the 1964 Baihe earthquake). Continued geodetic (GNSS, InSAR), seismic (dense array monitoring), and geological (borehole pressure measurements) investigations will be crucial for refining fault geometry, unraveling potential multi-fault ruptures, and improving forecasting models. Addressing data gaps, such as misfits at certain far-field GNSS stations, will further clarify the regional tectonics and aid in developing effective mitigation strategies to reduce seismic risk in southwestern Taiwan.

Author contributions

Y.S. wrote the main manuscript and prepared the figures. K.E.C. edited the manuscript. W.L.C., H.C.C., S.H.H., W.Y.L., E.J.L., R.Y.C., and C.L.C. reviewed the manuscript. All authors approved the final manuscript.

Data availability

No datasets were generated or analysed during the current study.

Declarations

Competing interests

The authors declare no competing interests.

Received: 25 February 2025 / Accepted: 28 March 2025
Published online: 11 April 2025

References

Avouac JP, Meng L, Wei S, Wang T, Ampuero JP (2015) Lower edge of locked main Himalayan thrust unzipped by the 2015 Gorkha earthquake. Nat Geosci 8(9):708–711

Biete C, Alvarez-Marron J, Brown D, Kuo-Chen H (2017) The structure of Southwest Taiwan: the development of a fold-and-thrust belt on a margins outer shelf and slope. Tectonics 37(7):1973–1993

Brown D, Alvarez-Marron J, Biete C, Kuo-Chen H, Camanni G, Ho CW (2017) How the structural architecture of the Eurasian continental margin affects the structure, seismicity, and topography of the South central Taiwan fold-and-thrust belt. Tectonics 36(7):1275–1294

Brown D, Alvarez-Marrón J, Camanni G, Biete C, Kuo-Chen H, Wu YM (2022) Structure of the south-central Taiwan fold-and-thrust belt: testing the viability of the model. Earth Sci Rev 231:104094

Ching KE, Rau RJ, Zeng Y (2007) Coseismic source model of the 2003 Mw 6.8 Chengkung earthquake, Taiwan, determined from GPS measurements. J Geophys Research: Solid Earth 112:B6

Ching KE, Johnson KM, Rau RJ, Chuang RY, Kuo LC, Leu PL (2011) Inferred fault geometry and slip distribution of the 2010 Jiashian, Taiwan, earthquake is consistent with a thick-skinned deformation model. Earth Planet Sci Lett 301(1–2):78–86

Ching KE, Gourley JR, Lee YH, Hsu SC, Chen KH, Chen CL (2016) Rapid deformation rates due to development of diapiric anticline in Southwestern Taiwan from geodetic observations. Tectonophysics 692:241–251

CWA (2025) Central Weather Administration - Earthquake Report. https://scweb.cwa.gov.tw/en-us/earthquake/data, accessed 4 February 2025

Huang MH, Tung H, Fielding EJ, Huang HH, Liang C, Huang C, Hu JC (2016) Multiple fault slip triggered above the 2016 Mw 6.4 MeiNong earthquake in Taiwan. Geophys Res Lett 43(14):7459–7467

Hubbard J, Almeida R, Foster A, Sapkota SN, Bürgi P, Tapponnier P (2016) Structural segmentation controlled the 2015 Mw 7.8 Gorkha earthquake rupture in Nepal. Geology 44(8):639–642

Le Béon M, Marc O, Suppe J, Huang MH, Huang ST, Chen WS (2019) Structure and deformation history of the rapidly growing Tainan anticline at the deformation front of the Taiwan mountain belt. Tectonics 38(9):3311–3334

Le Béon M, Chen CC, Huang WJ, Ching KE, Shih JW, Tseng YC, Chiou YW, Liu YC, Hsieh ML, Pathier E, Lu CH (2024) Aseismic deformation within fold-and-thrust belts: example from the Tsengwen river section of Southwest Taiwan. Geoscience Lett 11(1):57

Lee SJ, Liang WT, Cheng HW, Tu FS, Ma KF, Tsuruoka H, Kawakatsu H, Huang BS, Liu CC (2014a) Towards real-time regional earthquake simulation I: real-time moment tensor monitoring (RMT) for regional events in Taiwan. Geophys J Int 196(1):432–446

Lee SJ, Liu Q, Tromp J, Komatitsch D, Liang WT, Huang BS (2014b) Toward real-time regional earthquake simulation II: Real-time online earthquake simulation (ROS) of Taiwan earthquakes. J Asian Earth Sci 87:56–68

Lee Z, Chuang RY, Wang IT, Chen LS, Chang WL, Chiu CY, Ching KE, Guo SW, Chen CL (2025) Fast Report: Surface deformation associated with the 2025 Dapu earthquake. accepted by *Terrestrial, Atmospheric and Oceanic Sciences.*

Liao WY, Lee EJ, Rau RJ, Chen DY, Wen S, Ching KE, Liang WT (2025) Fast report: unveiling the seismogenic structure of the 2025 M6.4 Dapu earthquake sequence in Western Taiwan with a deep-learning-empowered earthquake catalog, submitted to *Terrestrial, atmospheric and oceanic sciences*

Lin I, Huang WC, Wang WH, Chiang CY, Wen S, Yeh YL, Chau-Huei C, Huang HC, Chen YN, Huang YC, Chang YZ (2025) Coexistence and Interplay of Thin-And Thick-Skinned Tectonics in Southwestern Taiwan: Insight from High-Resolution Seismicity Data. SSRN: https://ssrn.com/abstract=5117019 or https://doi.org/10.2139/ssrn.5117019

Mouthereau F, Lacombe O (2006) Inversion of the paleogene Chinese continental margin and thick-skinned deformation in the Western foreland of Taiwan. J Struct Geol 28(11):1977–1993

Mouthereau F, Lacombe O, Deffontaines B, Angelier J, Brusset S (2001) Deformation history of the Southwestern Taiwan foreland thrust belt: insights from tectono-sedimentary analyses and balanced cross-sections. Tectonophysics 333(1–2):293–322

Okada Y (1985) Surface deformation due to shear and tensile faults in a half-space. Bull Seismol Soc Am 75(4):1135–1154

Peng W, Chen KH, Toda S (2019) Evaluating the association between tectonic tremors and earthquakes in Taiwan from 7 years catalogs. J Geophys Research: Solid Earth 124(4):950–3965

Suppe J (1980) Imbricated structure of Western foothills belt, south-central Taiwan. Petroleum Geol Taiwan 17:1–16

Suppe J (1983) Geometry and kinematics of fault-bend folding. Am J Sci 283:684–721

Suppe J (1984) Kinematics of arc-continent collision, flipping of subduction and back-arc spreading near Taiwan. Mem Geol Soc China 6:21–33

Teng LS (1990) Geotectonic evolution of the late cenozoic arc-continent collision in Taiwan. Tectonophysics 183:57–76

USGS (2025) U.S. Geological Survey – Earthquake Hazards Program: Earthquakes. https://www.usgs.gov/programs/earthquake-hazards/earthquakes, accessed 4 212 February 2025

Wu FT, Rau RJ, Salzberg D (1997) Taiwan orogeny: thin-skinned or lithospheric collision? Tectonophysics 274(1–3):191–220

Wu Y-M, Hsu YJ, Chang C-H, Teng LSY, Nakamura M (2010) Temporal and Spatial variation of stress in Taiwan from 1991 to 2007: insights from compressive first motion focal mechanism catalog. Earth Planet Sci Lett 298:306–316

Wu YM, Lin YH, Yang BM, Ke SS (2025) Performance of the P-Alert real-time shakemaps system and onsite warning during the 2025 ML 6.4 Dapu earthquake, accepted by *Terrestrial, atmospheric and oceanic sciences*. https://doi.org/10.1007/s44195-025-00086-w

Yuan J, Huang ST, Chou TT, Wu JC, Lu DL (1987) On the origin of the abnormal pressure zones in the Southwestern Taiwan, *Annals of Exploration and Production (CPC).*, 10, 1–27

Publisher's note